

Dysprosium doped Copper Nanoferrites for Investigation of Structural, Magnetic, Optical and Morphological Properties

Sanchita V. Chavan¹, Vyankati R. Jadhav¹, Sunanda H. Pisal², Vishal H. Goswami³, Pradip B. Sarawade⁴, Ramesh B. Bhise⁵ and Mahendra S. Shinde^{6,*}

¹ PG Department of Physics, PDEA's Annasaheb Magar College, Hadpsar, Pune-28, Affiliated to Savitribai Phule Pune University, Pune, Maharashtra, India

² PG Department of Physics, RSS's S. M. Joshi College, Hadpsar, Pune-28, Affiliated to Savitribai Phule Pune University, Pune, Maharashtra, India

³ Department of Physics, Chikitsak Samuha's Sir Sitaram and Lady Shantabai Patkar College of Arts & Science and V. P. Varde College of Commerce & Economics, Goregaon West, Mumbai, Affiliated to University of Mumbai, Kalina, Maharashtra, India

⁴ Department of Physics, University of Mumbai, Kalina, Mumbai, Maharashtra, India

⁵ PG Department of Physics, Hon. Balasaheb Jadhav Arts, Commerce and Science College, Ale (Junnar), Pune – 412411, Affiliated to Savitribai Phule Pune University, Pune, Maharashtra, India

⁶ Department of Physics, M.J.M. Arts, Commerce and Science College, Karanjali (Peth) Nashik– 422208. Affiliated to Savitribai Phule Pune University, Pune, Maharashtra, India

Received: 27 Jul. 2024, Revised: 18 Feb. 2025, Accepted: 14 Mar. 2025

Published online: 1 May 2025

Abstract: In present study sol-gel autocombustion techniques were used to create Dysprosium (Dy^{3+}) doped Copper ferrites. Characterization of these produced compounds was done with XRD, SEM, FTIR, VSM, TG-DTA, and TEM. The TGA shows weight loss is caused by the autocatalytic oxidation reduction reactions of nitrates. Dy^{3+} doped in $Cu_xFe_{2-x}O_4$ ($x=0.00, 0.025, 0.05, 0.075, 0.1, 0.125$ and 0.15) exhibits a shape resembling fibrous reticulated grid. When Dy^{3+} concentration rises, the average grain size also rises. The XRD analysis of copper ferrite doped with Dy^{3+} exhibits a cubic spinel phase. The TEM investigation revealed that the particle size was between 30 to 40 nm. The FT-IR spectra displayed two prominent absorption bands at 540 cm^{-1} , which are indicative of the metal's intrinsic stretching vibrations at the tetrahedral site, and lowest band detected at 424 cm^{-1} corresponds to the octahedral site, while the co-tetrahedral site.

Keywords: Sol-gel Techniques, Dysprosium, Copper ferrites, Band gap, Cation Distribution, etc.

1. Introduction

Important magnetic compounds known as nanocrystalline ferrites have garnered a lot of interest lately because of their numerous technical and biological uses. The modification of structural characteristics including size, shape, and morphology is necessary for the wide range of applications of magnetic nanoparticles. Material scientists put a lot of work into modifying spinel ferrites' characteristics to meet the demands of particular applications. Ferrites' structural characteristics are greatly impacted by the preparation process, sintering conditions, cation substitution, and cation distribution [1-2]. Ferrite nanoparticles can be produced by a variety of physical and chemical techniques. Researchers became interested in the sol gel approach due to its benefits, which included producing nanoparticles with a narrow range, compact size, and superior chemical homogeneity [3-4]. It is recognized as the mineral tenorite, which has the characteristics of organic solvents, water dissolved, and red color. Copper (II) oxide functions as a semiconductor of the p-type [1]. It is designed to intensify the brightness of optical

equipment in order to produce dry battery cells as the cathode. Together with its narrow band gap, cupric oxide (CuO) is a necessary metal oxide transition that serves as the foundation for a number of high magneto-resistant materials and superconductors that can withstand high temperatures.

Since it is less expensive, requires less heat treatment at lower temperatures, and is easier to handle than other processes, sol-gel autocombustion is one of the most popular techniques for producing nanoscale ferrite powder [5]. Starting ingredients included Ferric nitrate $Fe(NO_3)_3 \cdot 9H_2O$ of analytical grade, Copper nitrate $Cu(NO_3)_2 \cdot 6H_2O$, Dysprosium nitrate $Dy(NO_3)_3 \cdot 5H_2O$, Citric acid $C_6H_8O_7 \cdot H_2O$, and ammonia solution ($NH_3 \cdot H_2O$). Sol gel auto-combustion was used to create two sets of five samples, each with a chemical formula of $CuFe_{2-x}O_4Dy_x$ ($x = 0.00, 0.025, 0.05, 0.075, 0.1, 0.125,$ and 0.15) nanoferrite particles. Metal nitrates function as an oxidizing agent and citric acid as a reducing agent. Citric acid functions as an organic fuel as well, giving the reactants a location to undergo redox reactions as they burn. The sol gel autocombustion is one of the widely used methods to prepare nanoscale ferrite powder

*Corresponding author E-mail: mahen3569@rediffmail.com

due to cost effective, low temperature heat treatment, and easy handling relative to other methods [6].

In this study, dysprosium doped copper ferrite was synthesized using the sol-gel auto combustion method [7]. The following properties were studied using various characterized techniques for synthesized ferrite materials: Structural behavior, Magnetic hysteresis, Band gap, Morphology, and Weight loss, Crystalline size, Cation distribution, etc. Catalytic activity of this copper doped with dysprosium. It was demonstrated that the rate constant in $\text{CuDy}_x\text{Fe}_2\text{O}_4$ [$x=0.00, 0.025, 0.05, 0.075, 0.1, 0.125, \text{ and } 0.15$] increases with an increase in the composition.

2. Materials and Methods:

2.1 Synthesis process:

As preliminary ingredients, extremely pure analytical reagent (AR) grade chemicals were used, such as iron (III) $[\text{Fe}(\text{NO}_3)_3 \cdot 9\text{H}_2\text{O}]$ nitrate nonahydrate, copper (II) $[\text{Cu}(\text{NO}_3)_2 \cdot 6\text{H}_2\text{O}]$ and dysprosium nitrate hexahydrate (III) $[\text{Dy}(\text{NO}_3)_3 \cdot 6\text{H}_2\text{O}]$ nitrate hexahydrate (99.99%). In order to create Dysprosiumdoped Copper ferrite powder, citric $(\text{C}_6\text{H}_8\text{O}_7)$ acid was selected as the fuel agent. The molar ratio of metal nitrates to citric acid was maintained at 1:1 using stoichiometric calculations. The mixture was put on a magnetic stirrer set to stir uniformly at 50 revolutions per minute. During the stirring process, ammonia (NH_3) solution was added to bring the pH level to 7 while keeping the temperature at 353 K. First, the mixture was made into a gel phase and subsequently underwent auto combustion burning to yield a loose, fluffy powder. To create a fine powder, the obtained powder was first calcined at 773 K for two hours, then sintered at 500°K for 5hrs and obtain a fine powder using characterization.

2.2 Characterization:

X-ray diffraction was used to analyze the structure and phase composition of the Dy–Cu ferrite nanoparticles. $\text{Cu-K}\alpha$ radiation ($\lambda = 0.15406 \text{ nm}$) was used. For every sample that was obtained, the Fourier transform infrared spectra analysis was performed to identify the chemical bonds. The spectrometer was used to record the data in the 400–4000 cm^{-1} wave number range. Field emission scanning electron microscopy (FESEM) were used to ascertain the morphology and chemistry of nanosize particles. The magnetic characteristics of the sample were measured using a vibrating sample magnetometer (VSM) at room temperature and an applied field of up to 10 k (Oe).

3. Result and Discussion:

3.1 XRD Analysis:

Figure-1 shows the $\text{CuFe}_{2-x}\text{O}_4\text{Dy}_x$ ($x = 0.00, 0.025, 0.05, 0.075, 0.1, 0.125, \text{ and } 0.15$) X-ray diffraction (XRD) pattern. All of the samples show the diffraction peaks corresponding to the planes (222), (400), (422), (433) and (532). It was

determined that every sample showed a cubic spinel structure. Samples containing more dysprosium show small peaks corresponding to the secondary phase. In addition to the pure spinel phase, rare earth doped systems might also have secondary phases. Bharathiet al. [8] revealed that the DyFeO_3 phase was present in the Dy-doped copper ferrite system. Compounds were synthesized and sintering at 400 °C for 5 hrs as determined by the X-ray diffraction (XRD) pattern.

Two theta ranges of room temperature to 80° were recorded for nanoferrite. The primary characteristic peak in the analysis of the XRD data for all samples was the formation of the cubic spinel structure. The lattice constant and crystalline size were computed using the reflection plane (400). The value derived from the XRD data analysis falls within the expected range of spinel cubic ferrites lattice constant [9].

Additionally, the successful replacement of rare earth Dy^{3+} cations with Fe^{3+} was confirmed by the presence of major XRD peaks at similar (though not identical) positions. It is evident from figure-1 that peak broadening occurs. This broadening results from the replacement of Fe^{3+} ions with Dy^{3+} ions, which involves f-orbitals, which are deeply buried and produce broad peaks instead of d-orbitals, which are exposed off and produce sharp peaks.

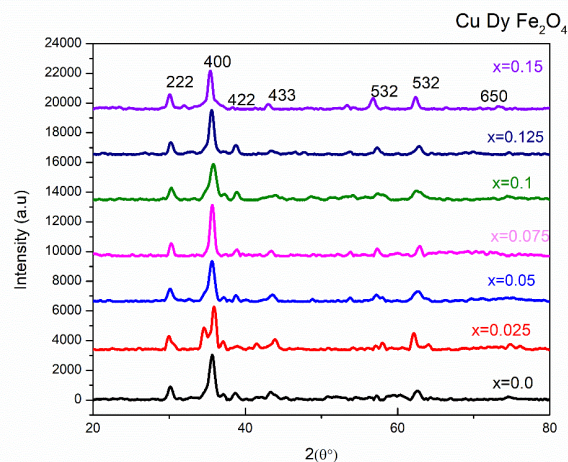


Fig. 1: XRD patterns of $\text{CuDy}_x\text{Fe}_{2-x}\text{O}_4$ ($x=0.00, 0.025, 0.05, 0.075, 0.1, 0.125$ and 0.15)

Table 1: Measured values of Lattice Parameter, X-ray and Dislocation Density, etc

Concentration of Dy(x)	Interplanar distance	Lattice Parameter(Å°)	X-ray Density	Crystalline Size(nm)	Micro Strain	Dislocation Density($\times 10^{14}$ line/ m^2)
0.000	2.5181	8.3527	5.4577	11.24	0.0033	0.0308
0.025	2.5835	8.5695	5.1080	11.91	0.0031	0.0267

0.500	2.5196	8.3575	5.5675	11.22	0.0033	0.0309
0.075	2.5154	8.3436	5.6562	15.25	0.0024	0.0167
0.100	2.5086	8.3211	5.7639	9.07	0.0041	0.0476
0.125	2.5209	8.3618	5.7407	12.62	0.0029	0.0244
0.150	2.5298	8.3915	5.7407	11.98	0.0031	0.0269

Using the ‘d’ value and appropriate (hkl) (400) parameters, the lattice constant ‘a’ was computed using the following formula:

$$A = d_{hkl} \sqrt{h^2 + k^2 + l^2} \tag{1}$$

All of the compounds' apparent particle sizes were estimated. By applying an analysis of the X-ray diffraction peak broadening Scherrer's equation [10]:

The cubic unit cell structure for $Cu Dy_x Fe_{2-x} O_4$ was obtained as

$$D = 0.9\lambda / \beta \cos(\theta) \tag{2}$$

Where,

λ is the radiation wavelength,

θ is the diffraction angle, and

β is the full width at half maximum (FWHM).

Table-1 shows the acquired lattice parameters.

Utilizing the relation below, one can compute the theoretical X-ray density:

$$D_{hkl} = \frac{8M}{Na^3} \tag{3}$$

in which N is the Avogadro's number, 'a' is the lattice constant, M is the molecular weight of the compound of ferrite sample, and 8 denotes the number of molecules per unit cell. Using the following relationship, one can determine the circular shape pellet's apparent density (experimental).

$$D = \frac{m}{v} = \frac{m_{\pi}}{r^2 h} \tag{4}$$

The mass, volume, radius, and thickness of the pellet are denoted by the letters. The sample's mass and symmetry are used to calculate the theoretical density of the samples, whereas the lattice constant and molecular weight determine the X-ray density. Table-1 makes it visible. Because of pores that are dependent on the sintering conditions, the X-ray density is higher than the apparent density [11].

3.2 SEM Analysis:

Samples are obtained, a morphology analysis is carried out, synthesized using the sol-gel concept, and it is demonstrated using scanning electron microscopy (SEM) technology. Figure-2 shows the pictures and the synthesis. According to [13], the agglomerated grain structure seen in the micrographs is caused by the interaction of magnetic nanoparticles.

It indicates a micrograph's irregular grain structure. The grain is described as having regular grain structure in the absence of voids and as being well-structured with no cracks [14]. It is well known that the image morphology is

comparable, horizontal, and less dispersed in terms of measurement. The SEM micrographs also show that as the Dy content rises, the grain size and porosity rise.

It is observed that the stoichiometric formula and the measured elemental ratios of compositions agree. The EDX spectrum showed that while the peak intensity of iron and nickel decreased, the peak intensity of dysprosium increased as the amount of Dy doped increased. It is evident from the EDX spectra that the prepared samples contain no extra impurities. The substitution sample peaks suggest that ions such as dysprosium and cobalt enter the ferrite structure [15].

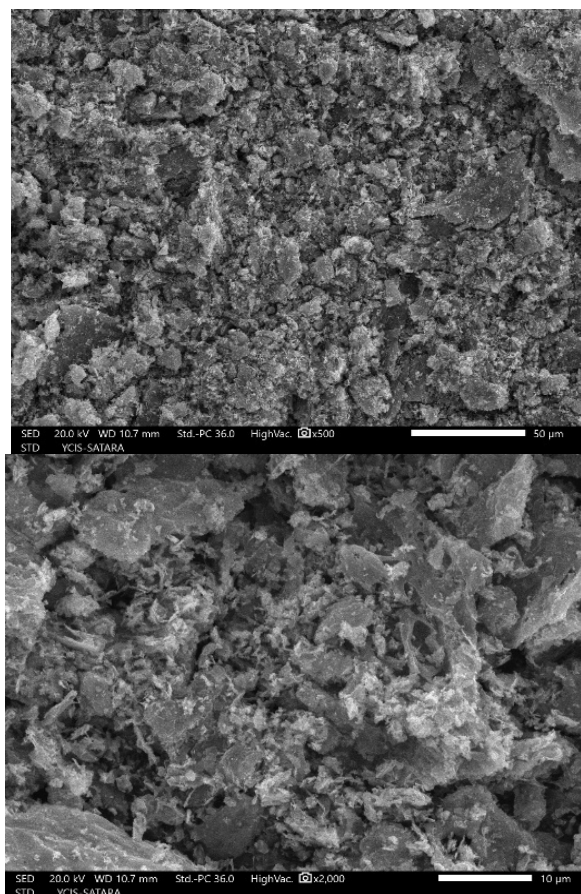


Fig. 2: Scanning Electron Microscopy (SEM) patterns of $Cu Dy_x Fe_{2-x} O_4$ ferrite nanoparticles

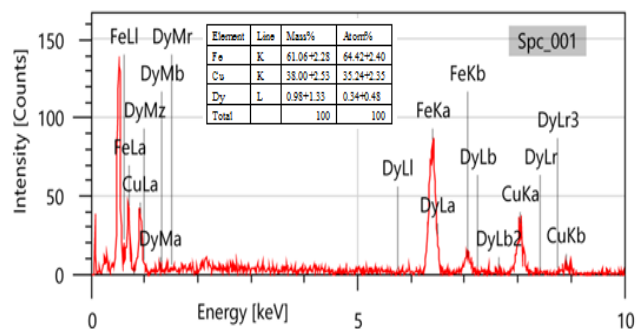


Fig. 2(c): EDAX spectrum and compositional data of $Cu Dy_x Fe_{2-x} O_4$ (x=0.075, 0.1) ferrite nanoparticles.

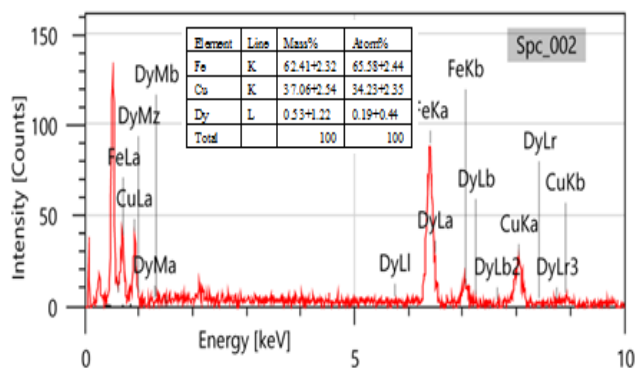


Fig. 2(d): EDAX spectrum and compositional data of $\text{CuDy}_x\text{Fe}_{2-x}\text{O}_4$ ferrite nanoparticles.

3.3 TEM Analysis:

Figure-3 shows TEM pictures of the $\text{CuDy}_x\text{Fe}_{2-x}\text{O}_4$ system nanoparticles with ($x=0.075, 0.1$). The TEM image revealed that these particles had not aggregated, and its measurement of 55 nm was found to be in close proximity to the value derived from the XRD pattern. The majority of the agglomerated nanoparticles have a spherical shape. The tendency of nanoparticles to aggregate in order to reach a low free energy state by decreasing the specific superficial area by lessening the interfaces with other particles may be the cause of the agglomeration of nanocrystals [12]. Table-1 displays the average particle size determined from the TEM images. The values obtained from XRD are nearly equivalent to the crystallite size.

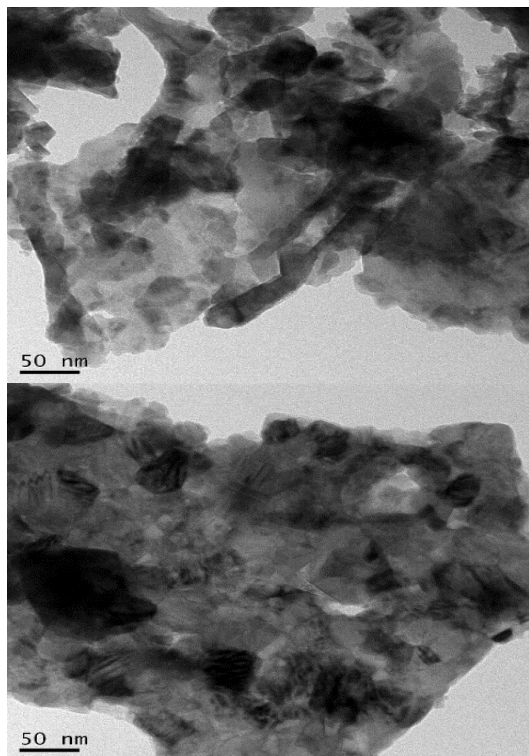


Fig. 3: Transmission Electron microscopy of $\text{CuDy}_x\text{Fe}_{2-x}\text{O}_4$ ferrite nanoparticles

3.4.VSM Analysis:

Figure-4 shows that magnetic hysteresis loop of $\text{CuDy}_x\text{Fe}_{2-x}\text{O}_4$ system ($x=0.00, 0.025, 0.05, 0.075, 0.1, 0.125$ and 0.15) were using vibrating sample magnetometer. The magnetic parameters such as saturation magnetization (M_s), Remanent magnetization (M_r), and Coercivity (H_c). The magnetic hysteresis loops characteristic of $\text{CuDy}_x\text{Fe}_{2-x}\text{O}_4$ system ($x=0.00, 0.025, 0.05, 0.075, 0.1, 0.125$ and 0.15) system are depicted in Figure-7, along with an inset that displays an enlarged area surrounding the origin. Evidently, at the maximum applied field, saturation magnetization is not attained. This could be because spins on nanoparticle surfaces are non-collinear, which makes spin alignment challenging even at high applied fields [16]. Table-2 lists each sample's saturation magnetization (M_s), Coercivity (H_c), and remnant ratio ($R=M_r/M_s$). For pure cobalt ferrite, the value M_s value has decreases from 96.8000 to 73.6000 emu/g and M_r value has decreased from 23.4400 to 7.0400 emu/g where the coercivity has increased from 58.3333 to 58.8889 Oe. The decrease of M_s with Dy content is consistent with the result reported for rare earth doped ferrites [17]. Tables demonstrate that the value of M_s is directly correlated with the size of the nanoferrite particles [18].

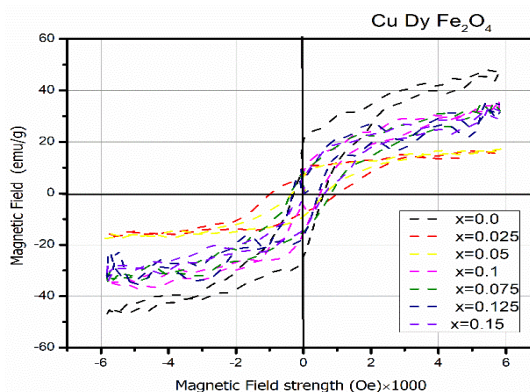


Fig. 4: Hysteresis loop of $\text{CuDy}_x\text{Fe}_{2-x}\text{O}_4$ samples at room temperature.

Table 2: Measured parameters for Magnetic parameters from Hysteresis loops

Content(x)	Coercivity (Hc)(Oe)	Remnant Magnetization (Mr)(emu/g)	Ms(emu/g)
0.0	058.3333	023.4400	096.8000
0.025	052.7778	011.0154	034.8308
0.05	052.7778	007.3143	036.471
0.075	042.7778	008.0800	074.4000
0.1	048.8889	008.5600	073.4400
0.125	058.8889	003.6800	073.6000
0.15	056.1111	007.0400	070.0800

Grain size, Cation distribution between the tetrahedral (A) and octahedral (B) sites, and preparation conditions all affect the saturation magnetization of ferrite material. The saturation magnetization may also be impacted by

modifications to the ion concentration and type in the A and B sites. The weakening of AB interactions may be the cause of the decrease in M_s with dysprosium content. The unpaired electrons of the ions occupying the A and B sites can interact in three different ways. However, Compared to A-A and B-B interactions, the A-B interaction is more common. The difference between the moments of the B and A sublattices in a ferrimagnetic material is called the net magnetic moment. On the spinel lattice's octahedral site, Dy^{3+} ions are substituted because of the large ionic radii. As a result, the substitution of Dy^{3+} ions for Fe^{3+} ions lowers the magnetic moment of the octahedral sublattice and the Fe^{3+} - Fe^{3+} interactions. M_s to drop off. Further, the ordering of the magnetic moments of rare earth ions takes place at very low temperatures and is primarily caused by the 4f electrons [19][20].

3.5.TG-DTAAnalysis:

Figure-5 displays the thermogram of the unannealed sample of $CuDy_xFe_{2-x}O_4$ system ($x=0.00, 0.025, 0.05, 0.075, 0.1, 0.125$ and 0.15). This thermogram indicates that the weight loss happened gradually. The desorption of adsorbed water in the samples is displayed in the first stage. Weight loss occurs during the second stage, which is caused by the hydroxides changing into the ferrite sample's oxides. The development of the spinel structure is said to be responsible for the third and final stage. Our group has published comparable thermogravimetric results for ferrite and perovskite nanoparticles [21,22].

According to the TG-DTA study (Figure-3), weight loss for 0.11% at Dy^{3+} doped Cu-ferrite 1.6%, 2.6%, 1.8% between, and negligible beyond Mass loss up to 200 °C is attributed to sample dehydration, whereas mass loss up to 600 °C is caused by organic materials and certain impurities evaporating. seven exothermic peaks can be seen in the DTA curve in the vicinity of 100 °C, 260 °C, 450 °C, and 800 °C. These peaks correspond to the evaporation of water molecules, the decay of organic molecules, and the phase formation of (0.11%) [23].

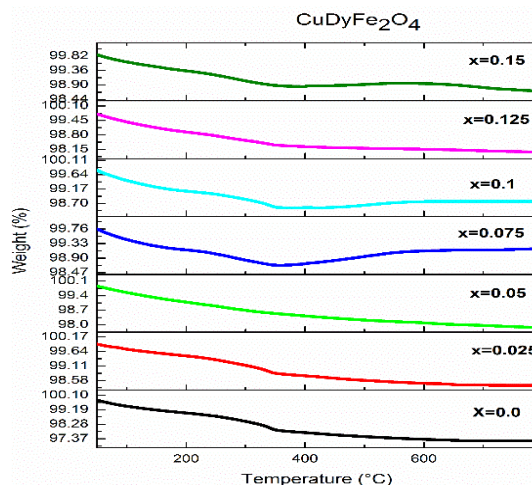
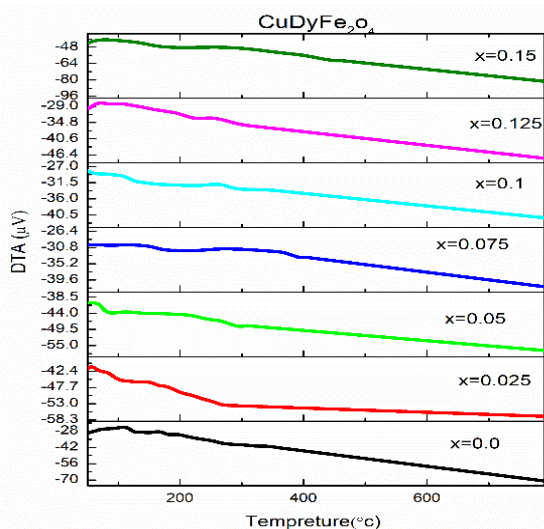


Fig. 5: (A) TGA and (B) DTA Curves of Dy^{3+} -doping $CuFe_2O_4$ nanoferrite

3.6 FT-IR Spectroscopy Analysis:

Typically, the infrared bands of solids are attributed to the vibration of ions within the crystal lattice within the wave range of $4000-500\text{ cm}^{-1}$. All spinel ferrites have two distinct metal-oxygen bands visible in their infrared spectra. Tetrahedral site (A) and octahedral site (B) are where the vibrations of the cubic spinel unit cell can be constructed, according to Waldron [24, 25].

The presence of distinctive absorption bands in the Fourier Transform Infrared (FT-IR) spectrum indicates the formation of spinel structure in the prepared samples. Fig. 6, provides the IR bands' vibrational frequencies. The bands of absorption seen in our spinel ferrites, the ranges $540-532\text{ cm}^{-1}$ and $408-424\text{ cm}^{-1}$ are characteristic. The lower frequency band (2) is brought on by the metal-oxygen vibration in the octahedral site, while the higher frequency band (1) corresponds to intrinsic stretching vibrations of the metal at the tetrahedral site [26].

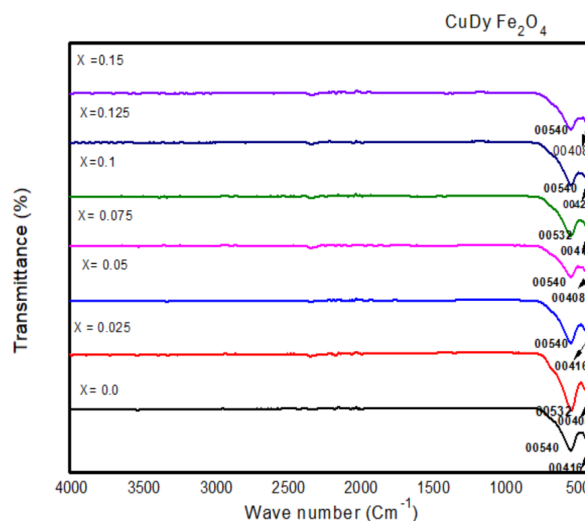


Fig. 6: FT-IR curve of Dy^{3+} doping $CuFe_2O_4$ nanoferrite

3.7 UV-Visible Spectroscopy Analysis:

The Dy³⁺doped copper ferrite optical absorption spectra have been investigated in the 200–800 nm wavelength range (Figure-7). In general, dopant element concentration, lattice strain, surficial impact, lattice structure parameters, and grain size all affect a material's optical band gap. The optical band gaps for samples owing to the first and second absorption bands were found using UV-Vis spectroscopy.

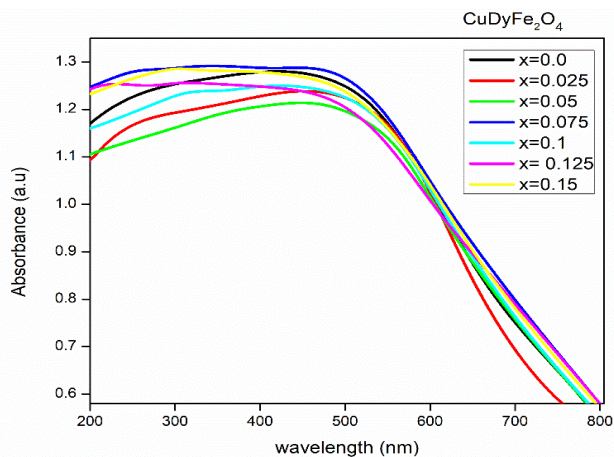


Fig. 7: Absorbance spectra CuDyFe₂O₄

The following formula can be used to determine the optical band gap based on the evolution of the α -coefficient as a function of incident photon energy. From 1.08 to 1.9, the absorbance increased quickly, with the maximum absorbance occurring at 543 nm wavelength. The formula is used to find the band gap energy.

$$\text{Band gap for energy} = 1240/\pi(\text{nm}) \quad (5)$$

4. Conclusion:

X-ray diffraction patterns show that the cubic spinel phase has formed without the presence of any extra impurity peaks, indicating that the sol-gel synthesis of CuDyFe₂O₄ (x=0.00, 0.025, 0.05, 0.075, 0.1, 0.125 and 0.15) compounds have been successfully completed and is sintering at 500°C. The XRD data yielded an average crystallite size of between 9.07 and 15.25 nm. At room temperature, all of the samples exhibit noticeable hysteresis and good saturation magnetization values. The octahedral site occupancy of Dy³⁺ ions is indicated by the FT-IR spectra. Dysprosium substitution reduces saturation magnetization and coercivity of copper ferrite, but the decrease in the latter is more pronounced. The coercivity in the multidomain regime is dependent on particle size, which explains the monotonic decline in coercivity with Dy³⁺ substitution. Because there is less A-B interaction when dysprosium ions are added to copper ferrite, saturation magnetization is reduced. These findings imply that copper ferrite nanoparticles' structural and magnetic characteristics can be adjusted to suit technological uses by substituting a proper quantity of dysprosium ions.

References

- [1] A. Goldman, Modern Ferrite Technology, New York: Van Nostrand Reinhold, 1990.
- [2] B. P. Jacob, S. Thankachan, S. Xavier, E. M. Mohammed, "Effect of Tb³⁺ substitution on structural, electrical and magnetic properties of Sol-gel synthesized nanocrystalline nickel ferrite", J. Alloys comp., Vol-578, 2013, pp314 – 9.
- [3] Jacob BP, Thankachan S, Xavier S, Mohammed EM. Dielectric behaviour and AC conductivity of Tb³⁺ doped Ni_{0.4}Zn_{0.6}Fe₂O₄ nanoparticles. J Alloys compound, Vol-54, 2012, pp29-35.
- [4] S. Thankachan, B. P. Jacob, S. Xavier, E. M. Mohammed, "Effect of samarium substitution on structural and magnetic properties of magnesium ferrite nanoparticles", J. Magn. Mater., Vol-348, 2013, pp140-5.
- [5] V. SalimianRizi, F. Sharifianjazi, H. Jafarikhorami, N. Parvin, L. SaeiFard, M. Irani, A. Esmailkhanian, "Sol-gel derived SnO₂/Ag₂O ceramic nanocomposite for H₂ gas sensing applications, Materials Research Express, Vol-6, 2019, pp1150-1152.
- [6] N. Sanpo, C. B. Christopher, W. Cuie, W. James, "Transition metal substituted cobalt ferrite nanoparticles for biomedical applications", Acta Biomater, Vol-9, 2013, pp5830-7.
- [7] S. E. Jacobo, S. Duhalde, H. R. Bartorello, J. Magn. Mater., 2004, 272–276, pp2253.
- [8] K. K. Bharathi, K. Balamurugan, P. N. Santhosh, M. Pattabiraman, G. Markadeyulu, "Magneto capacitance in Dy doped Ni ferrite", Phy. Rev B, Vol-77, 2008, pp172401 -4.
- [9] A. A. Satar, H. M. El-Sayed, K. M. El-Shokrofy, M. M. El-Tabey, J. Appl. Sci., Vol-5, 2005, pp162.
- [10] B. D. Cullity, S. R. Stock, "Elements of X-Ray Diffraction", 3rd ed., Prentice Hall, New York, 2001.
- [11] M. A. Gabal, S. S. Ata-Allah, Mater. Chem. Phys., Vol-85, 2004, pp104.
- [12] Sheena Xaviera, Rintu Mary Sebastianb, and E. M. Mohammedb, "Effect of dysprosium substitution on structural and magnetic properties of cobalt ferrite nanoparticles", International Journal of Engineering Science and Innovative Technology (IJESIT), Vol-4, 2015.
- [13] Aurelija GATELYTĖ, "Sol-Gel Synthesis and Characterization of Selected Transition Metal Nanoferrites", Materials Science (MEDŽIAGOTYRA), Vol-17, Issue-3, 2011.
- [14] M. K. Kokare, N. A. Jadhav, V. Singh, S. M. Rathod,

- Opt. Laser Technology, Vol-112, 2019, pp107.
- [15] L. Chauhan, N. Singh, A. Dhar, H. Kumar, S. Kumar, K. Sreenivas, *Ceram. Int.*, Vol- 43, 2017, pp8378.
- [16] P. Priyadarshini, A. Pradeep, P. S. Rao, G. Chandrasekharan, "Structural, spectroscopic and magnetic study of nanocrystalline Ni-Zn ferrite", *Mater Chem. Phys.*, Vol-116, 2009; pp207-13.
- [17] J. Peng J, M. Hojamberdiev, Y. Xu, B. Cao, J. Wang, H. Wu, "Hydrothermal synthesis and magnetic properties of gadolinium-doped CoFe_2O_4 nanoparticles", *J.Magn.Magn. Mater*, Vol-323, 2011, pp133-8.
- [18] Alex Goldman, *Modern Ferrite Technology*, 2nd Ed., Springer, Pittsburgh, 2006.
- [19] A. Nikzad, R. Parvizi, G. Rezaei, B. Vaseghi, R. Khordad, *J. Electron. Mater.*, Vol-47, 2018, pp1302.
- [20] A. A. Kadam, S.S. Shinde, S.P. Yadav, P.S. Patil, K.Y.Rajpure, *J. Magn. Magn. Mater.*, Vol-329(59), 2013.
- [21] Z. Anwar, M. Azhar Khan, A. Mahmood, M. Asghar, I. Shakir, M. Shahid, I. Bibi, M. Farooq Warsi, *Journal of Magnetism and Magnetic Materials*, Vol-355(169), 2014.
- [22] M. Ejaz, A. Mahmood, M.A. Khan, A. Hussain, A. Sultan, A. Mahmood, A.H. Chughtai, M.N. Ashiq, M.F. Warsi, I. Shakir, *Journal of Magnetism and Magnetic Materials*, Vol-404(257), 2016.
- [23] Maheshwary, B. P. Singh and R. A. Singh, *New J. Chem.*, Vol-39, 2015, pp4494.
- [24] R. D. Waldron, "Infrared spectra of ferrites", *Phy Rev*, Vol-99, 1955, pp1727-35.
- [25] J. Feng, R. Xiong, L. Cheng, Y. Liu, *J. Supercond. Nov. Magn.*, Vol-30, 2017, pp3513
- [26] M. Srivastava, S. Chaubey, A.K. Ojha, *Mater. Chem. Phys.*, Vol-118, 2009, pp174.